OPO OPHTHALMIC & PHYSIOLOGICAL OPTICS
THE JOURNAL OF THE COLLEGE OF OPTOMETRISTS

Ophthalmic & Physiological Optics ISSN 0275-5408

Evaluating glaucomatous abnormality in peripapillary optical coherence tomography enface visualisation of the retinal nerve fibre layer reflectance

Bright S. Ashimatey, Brett J. King, Stephen A. Burns and William H. Swanson

Indiana University School of Optometry, Bloomington, USA

Citation information: Ashimatey BS, King BJ, Burns SA & Swanson WH. Evaluating glaucomatous abnormality in peripapillary optical coherence tomography enface visualisation of the retinal nerve fibre layer reflectance. *Ophthalmic Physiol Opt* 2018; 38: 376–388. https://doi.org/10.1111/opo.12449

Keywords: enface image, glaucoma, optical coherence tomography, reflectance, retinal nerve fibre bundle

Correspondence: William H Swanson
E-mail address: wilswans@indiana.edu

Received: 16 November 2017; Accepted: 20 February 2018; Published Online: 30 March 2018

Abstract

Purpose: Optical coherence tomography (OCT) enface visualisation of the retinal nerve fibre layer (RNFL) reflectance has been found to have some advantages over retinal thickness measures. However, it is not yet clear how abnormalities on enface images relate to findings of abnormalities from other clinical measures such as the circumpapillary retinal nerve fibre layer thickness (cRNFLT). We developed a technique to analyse the RNFL reflectance on the OCT enface images, and to investigate its relation with the cRNFLT.

Methods: Spectralis (www.heidelbergengineering.com) OCT scans of the central retinal ±24° were analysed in the study eye of 31 controls and 33 patients, ages 61 (±9) and 69 (±8) years respectively. Enface slab-images were extracted at 16–24, 24–36, and 24–52 μm from the inner limiting membrane in the temporal raphe, perifoveal and disc regions respectively. Reflectance probability maps were generated for the patients based on the control data. Glaucomatous abnormality was defined on the slab-images when the slab-area with reflectance abnormality was greater than the 95th percentile, and on the cRNFLT when the thickness measure was less than the fifth percentile, of that found in controls. The fraction of slab-image showing reflectance abnormality was compared to cRNFLT in the patient group, using Spearman's rho. Agreement between the findings of abnormality based on cRNFLT and slab-image reflectance was assessed using Cohen's kappa.

Results: Slab-image and cRNFLT findings were in agreement for 26/33 eyes; four subjects showed cRNFLT abnormality but not slab-image abnormality, and three subjects showed slab-image abnormality but not cRNFLT abnormality. Spearman's rho found $r_s(31) = -0.82$. The reflectance findings and cRNFLT findings were consistent in 27/33 for both the superior temporal (ST) and inferior temporal (IT) sectors, and Cohen's kappa found 0.53 and 0.61 respectively.

Conclusion: The surface area of enface slab-images showing RNFL reflectance were strongly related to the cRNFLT measures, and the classification of a subject with glaucoma based on enface reflectance findings and cRNFLT findings had a generally good agreement. The larger retinal area assessed by the enface method preserves the spatial location of the RNFL abnormalities, and makes the technique a useful approach for identifying regions of potential RNFL abnormality for targeted perimetry.

Introduction

Structural evaluation of the retinal nerve fibre layer (RNFL) is a key component of glaucoma assessment. Recent years have seen dramatic improvements in imaging technologies for assessing the structural integrity of the ganglion cells, retinal nerve fibre layer and disc morphology.[1] One of these includes optical coherence tomography (OCT) enface visualisation of RNFL reflectance.[2–5] Unless constrained by the shape of the eye, the enface technique enables the visualisation of the RNFL over a large retinal area with a 7 μm axial resolution. Compared to the circumpapillary retinal nerve fibre layer thickness (cRNFLT) – one of the most commonly used structural assessment techniques – the large retinal area assessed by the enface technique presents the clinician with the ability to diagnose glaucoma by evaluating variations in the RNFL across the retina. The large retinal area assessed by the enface technique also makes it more robust to the effects of axial length,[6] segmentation errors, and other source of artefacts that affect the cRNFLT findings.

Recent work by Hood and colleagues found that the details of glaucomatous abnormalities were better seen on RNFL enface reflectance images than on the thickness maps.[2] Furthermore, Alluwimi *et al.*[7] have demonstrated that the spatial detail of the glaucomatous abnormalities seen on the enface reflectance findings can be successfully used to guide perimetric sampling for assessing glaucomatous vision loss. It has also been shown in a rat model that the RNFL reflectances assessed by the enface technique decrease at the onset of nerve fibre degeneration, preceding the loss in thickness measure assessed by the cRNFLT protocol.[8] Despite the prospects of enface visualisation of the RNFL reflectance, it is not yet clear how glaucomatous abnormality on the enface images is to be defined in a clinical population. It is also not clear how the reflectance abnormalities on the enface images compare with abnormalities from other structural measures already in use for patient care. There is even the concern that the highly directional reflectivity of the nerve fibre bundles[9,10] could affect evaluation of enface reflectance abnormalities.

To enhance the interpretation of the RNFL reflectances on the enface images, and to assess its role in patient care, it is necessary to understand how the reflectance findings on the enface images relate to the findings of glaucoma assessment techniques already in clinical use, such as cRNFLT. The nature of this relation can provide some useful cues as to how glaucomatous abnormalities on the enface images can be defined.

In this study we developed and applied a quantifying technique to assess RNFL reflectance abnormalities on enface images. In the technique, we adapted strategies to mitigate the impact of the between-subject variability in the retinal anatomical features, and reflectance artefacts such as presumed glial alteration reflectances[11–13] on quantifying the RNFL enface images. The findings of reflectance abnormalities on the enface images were compared to the glaucomatous abnormalities assessed with the cRNFLT protocol. The nature of the relationship between the two measures has provided some useful information on how the reflectance abnormalities on the OCT enface images relate to cRNFLT measures, and also provided guidance on how glaucomatous abnormalities can be identified on the enface images.

Methods

Subjects

We analysed OCT volume scans acquired in the study eye of 31 controls free from eye disease, and from 33 patients with glaucoma enrolled in our lab for an ongoing research project investigating the structure of the retinal nerve fibre layer in OCT imaging. The controls and patients were recruited from the pool of subjects who visited the Indiana University School of Optometry, Bloomington eye clinic.

Inclusion and exclusion criteria

Inclusion criteria were best-corrected visual acuity of at least 20/40 (0.30 logMAR, 6/12), refractive corrections between +6 and −9 dioptre spherical equivalent and cylindrical correction within ±3.0 dioptres, and clear ocular media. Control subjects were required to have had normal results from a comprehensive eye exam (not more than two years before the study) that included clinical evaluation of the disc and RNFL. Patients with glaucoma had normal retinal findings with the exception of disc, RNFL, and perimetric abnormalities associated with glaucoma, and were under the care of an eye care practitioner. Perimetric visual field results were considered as showing glaucomatous abnormality when the total (or pattern) deviation maps had reproducible defects at two or more contiguous points with $p < 0.01$, or three or more contiguous points with $p < 0.05$, or a 10-dB difference across the nasal horizontal midline in the presence of clinical glaucomatous optic neuropathy.[14] Exclusion criteria were ocular or systemic disease, other than glaucoma, currently affecting visual function. Eyes with epiretinal membranes were also excluded.

Study protocol

Written, informed consent was obtained after explaining the nature and purpose of the study to the participant. The subject's visual acuity was checked and high density images were acquired with the Spectralis OCT (www.heidelbergengineering.com). This research project followed the tenets

of the Declaration of Helsinki and was approved by the Indiana University Institutional Review Board (IRB).

Imaging protocol

The retinal images and cRNFLT measures were acquired with Spectralis OCT. The cRNFLT measures were obtained along the circumference of a 12° diameter circle centred on the optic disc using the Spectralis device cRNFLT protocol.

A retinal area approximately corresponding to the central ±24° was imaged. Six OCT volumetric scans were acquired and then montaged to cover the intended retinal region (*Figure 1*). In 10 subjects (imaged with an earlier version of the research protocol), the region temporal to the fovea (*Figure 1c*) was imaged in a single OCT scan session. One trained optometric technician acquired all the images. High speed imaging mode setting (with nominal spacing of 11 μm between a-scans) was used and the spacing between b-scans was set to 30 μm. Each b-scan was averaged over nine frames. The images acquired from each subject were montaged using customised montaging software written in MATLAB (www.mathworks.com). Regions of overlap between images were represented by the highest pixel value of the two images being montaged.

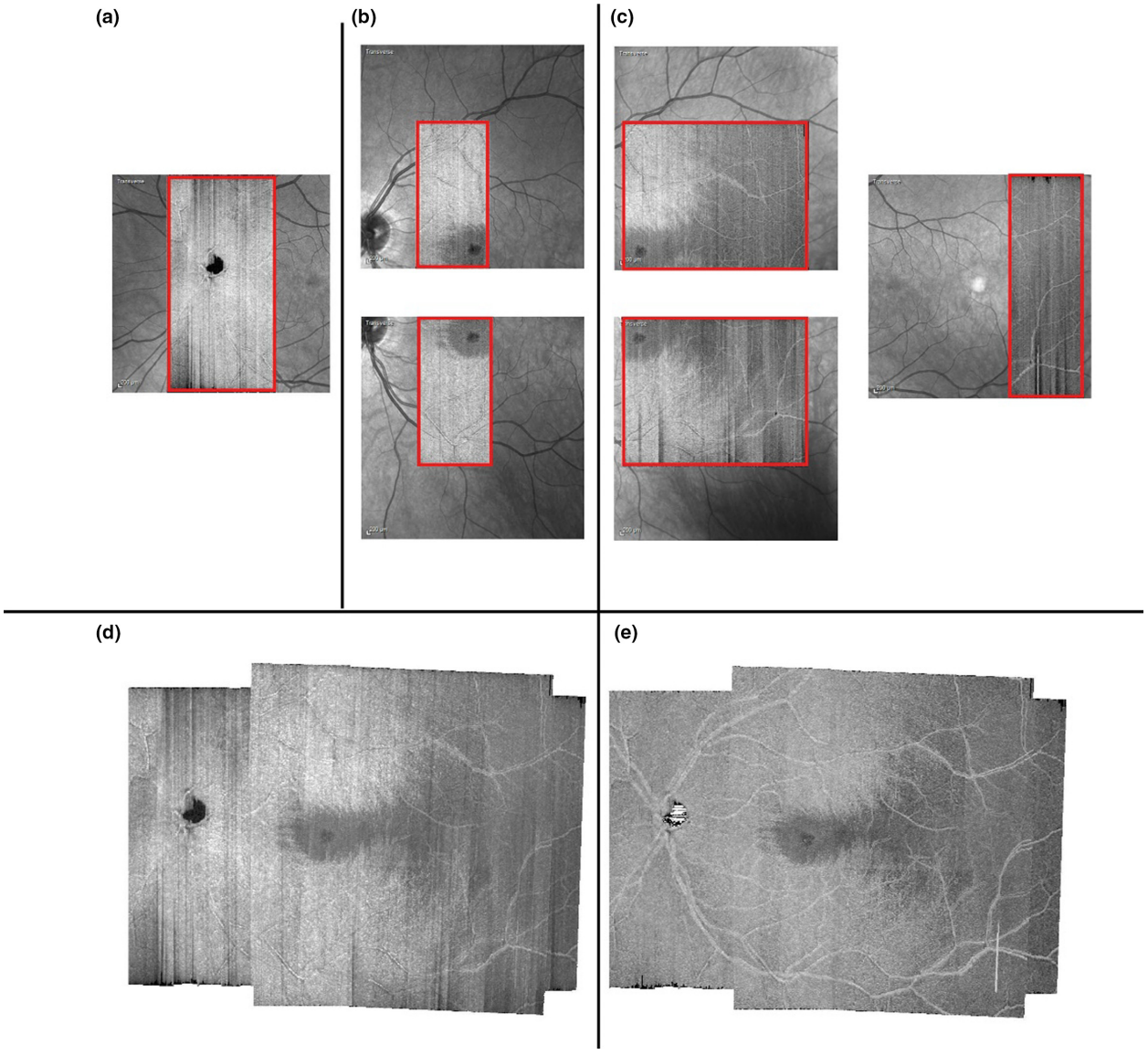

Figure 1. Retinal region imaged. (a–c) Illustrate the six individual OCT images acquired in a subject. The regions in red show the OCT scans superimposed on their respective Scanning Laser Ophthalmoscope (SLO) images. (d) a montage of the individual OCT images; (e) a montage of the attenuation coefficient maps (see text for details). (d) and (e) are 4 μm thick slab-images extracted from 20–24 μm beneath the inner limiting membrane.

Image processing

The OCT scans were processed to compensate for reflectance artefacts from vitreal floaters or low quality b-scans using a method proposed by Vermeer *et al.* and Girard *et al.*[15,16] In brief, the method is used to replace the measured brightness by an estimate of the attenuation of light as it is propagated through the retinal layers. The approach is based on the assumption that most of the light reaching the retina is attenuated by scattering. The method can be explained by two principles. First, the amount of light from any given retinal depth Z received by the detector is a constant proportion of the total amount of light scattered at that point. Second, the fraction of the light arriving at Z, which is scattered, is a measure of the intrinsic scattering property of the retinal cells at Z, and is independent of the amount of light arriving at that depth. The approach therefore presents a method for extracting the intrinsic reflectance properties of the retinal layers, and can mitigate the impact of the variations in the intensity of light reaching the retina or the signal strength of the light received at the detector. Equation 17 in Vermeer *et al.*[15] was used to construct the attenuation coefficient maps from the OCT scans. In Vermeer *et al.* the equation 17 was further simplified to derive equation 18, which is similar to equation A3 in the appendix of Girard *et al.*[16] In both Vermeer *et al.* and Girard *et al.*, the methods were developed for compensating for the shadowing effects of retinal vessels on the layers beneath the vessels, but the method is also suitable for compensating for other reflectance artefacts in OCT enface visualisation of the RNFL reflectance. An example of the processed vs unprocessed OCT images is shown in *Figure 1*.

OCT enface slab-image extracting

Enface reflectance slab-images were extracted by averaging the voxels within the OCT volume scan. Three types of slab-images were extracted. In the first, slab-images were extracted as 52 μm thick sections starting from the inner limiting membrane (ILM)/vitreous interface (0 μm) and terminating at 52 μm below the ILM, as in Hood *et al.*[2] In the second, we emphasised the reflectances from the retinal structures presumed to be glial cell alteration[11–13] by extracting 4 μm thick slab-images from 10 μm to 14 μm below the ILM (shown in *Figure 2*). In the third, slab-images were extracted using depth parameters customised to mitigate the impact of the putative glial alteration reflectances (*Figure 2*) on visualising/quantifying the RNFB reflectance. For these customised slab-images, we varied the thickness of the slab-images, and the depth (from the ILM/vitreous interface) at which they began. The slab-image in the disc region (*Figure 1a*) was generated at 24–52 μm. The slab-image in the quasi-perifoveal region (*Figure 1b*) was generated at 24–36 μm, and that in the quasi-raphe (*Figure 1c*) was generated at 16–24 μm. From a preliminary analysis, we determined that the slab-images generated at these depths mitigated the impact of the putative glial alteration reflectances on visualisation of the RNFB reflectances (when RNFBs were present). Examples from three patients with putative glial alterations are shown in *Figure 2*.

Quantifying the enface abnormalities

A thresholding technique was applied to transform the slab-image pixel values. First, a background attenuation coefficient (potentially from the endfeet of the Müller cells) was computed at 36 μm depth below a region approximating the triangular area of the temporal raphe,[3,17,18] where RNFBs are expected to be absent at this depth. The background value was used to threshold the slab-image – after the slab-image was extracted – setting the pixel value to zero (0) in regions of the slab-image where the RNFBs were not visible. In a second step, a grid of 20-pixel-by-20-pixel boxes was superimposed on the image starting from the foveal reflex and progressing towards the disc. The region temporal to the fovea – the temporal raphe – was not analysed because the reflectances from the presumed glial proliferations were still apparent. In addition, the spacing of the b-scans for the imaging protocol used in this study was not optimal for assessing the raphe; elsewhere,[19] a more suitable imaging protocol for assessing the raphe has been proposed. Some regions nasal to the fovea were not analysed, and were considered to be unreliable, due to the high between-subject variability in the RNFL reflectance at those regions. These regions included the areas around the fovea where no RNFL reflectances were present due to the ganglion cell displacements, and regions approximating the disc area.

The box size of the grid superimposed on the images was determined based on a preliminary analysis of the data in which we found that smaller grid-boxes were efficient at localising wedge defects, but yielded high between-subject variability in the control population, while larger grid-boxes had low between-subject variability but were not efficient for localising wedge defects. The attenuation coefficient values within each grid box were averaged and scaled to a ratio index by dividing the average by 255 (the highest pixel value possible). We compensated for between-subject variability in the disc-fovea angle by aligning the grid along the disc-fovea angle.

Quantifying retinal nerve fibre layer reflectance abnormality on the enface slab-images

Lower normative reference data for each box within the grid were computed as the mean – 1.64*standard

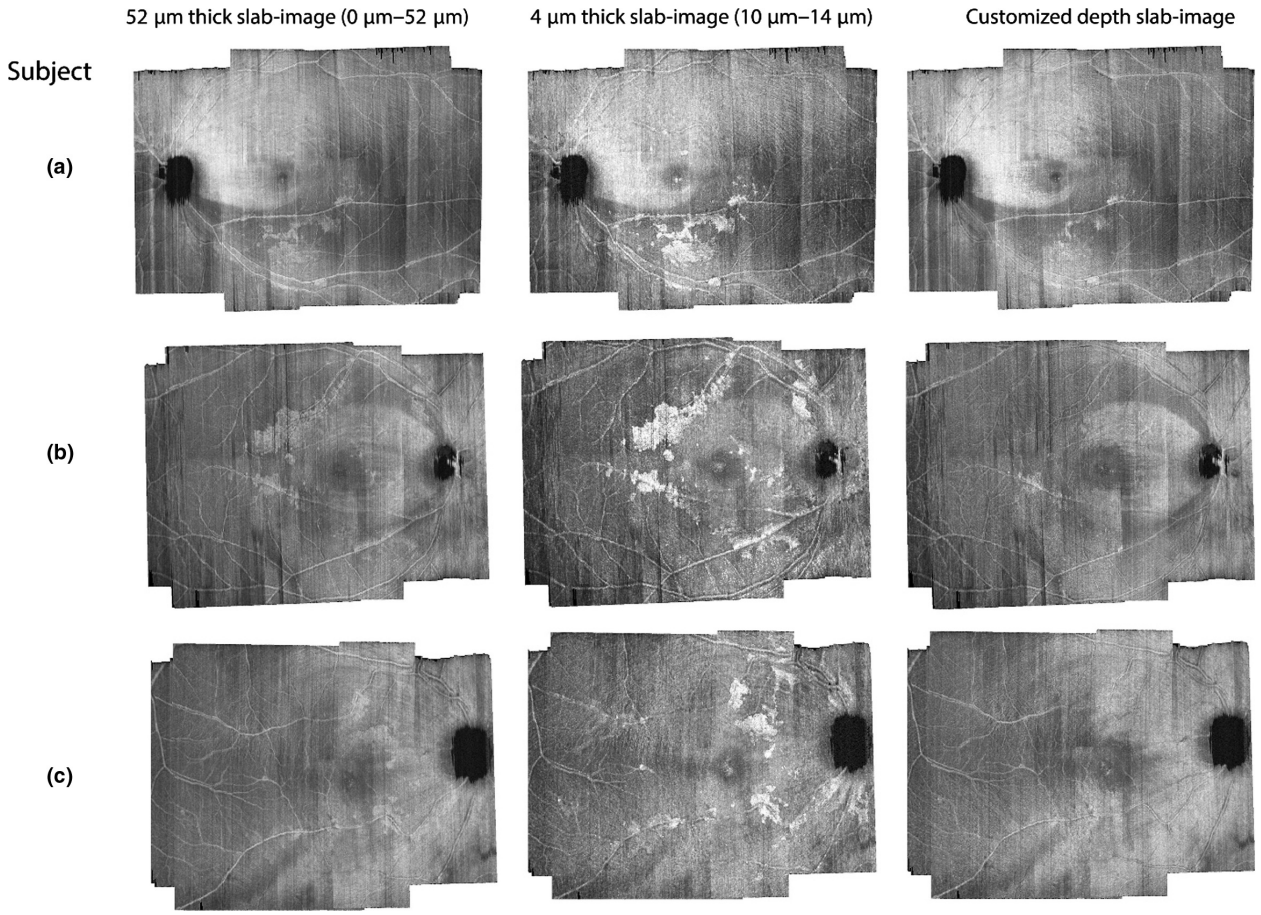

Figure 2. Axial sampling of OCT volume scans to mitigate the impact of putative proliferated glia (appearing as patchy reflectances) on visualising/quantifying the RNFB reflectance. The first column shows the enface slab-images for three patients with glaucoma extracted using the slab-image parameters used by Hood *et al*. The second column shows 4 µm thick slab-images for the patients, extracted to highlight the putative glial alterations seen as patchy glittering[13] reflecting structures. The third column shows the customised slab-images that mitigate the impact of the reflecting glia on visualising the RNFB reflectance.

deviation (S.D.) and mean − 2.34*S.D. representing fifth and first percentiles respectively, assuming a Gaussian distribution for the control data. A box within the grid was identified as showing abnormality when the reflectance finding was lower than the first percentile of the normative data.

We quantified abnormality on the enface slab-images as the fraction of grid-boxes flagged as showing reflectance abnormality in the enface region under consideration.

Quantifying circumpapillary retina nerve fibre layer thickness abnormality

We computed the degree of cRNFLT abnormality using a ratio metric we termed depth of defect (DD). Mathematically, the depth of defect was computed as

$$\mathrm{DD} = \frac{(A - B)}{B}$$

where A is the cRNFLT measure of the sector under consideration and B is the mean normal cRNFLT reported by the machine for the patient's age and the sector under consideration.

Our goal was to understand how the enface reflectance abnormalities related to the severity of glaucomatous abnormalities assessed with the cRNFLT protocol. Computing the depth of the defect allowed us to normalise the severity of the glaucomatous abnormality quantified in a subject based on the subject's age. This also provided a way of expressing the severity of the glaucomatous abnormality on a ratio-scale in a manner similar to the reflectance findings.

Analysis

The reflectance findings and the cRNFLT measures, in the patients with glaucoma, were compared using Spearman's rho. We first compared the reflectance abnormality findings for the entire enface area to findings for the temporal half of the cRNFLT measure – computed as the weighted sum of the thickness measures from inferior temporal (IT), superior temporal (ST) and temporal (T) disc sectors. Secondly, we compared the reflectance findings in the superior and inferior halves of the enface slab-image, to the IT and superior temporal ST cRNFLT respectively.

We computed absolute agreement to compare the categorisation of the cRNFLT sector and reflectance findings, and computed Cohen's kappa statistic. We compared the agreement between abnormality in the superior halves and inferior halves of the enface slab-image, with cRNFLT abnormality findings for ST and IT sectors respectively. Glaucomatous abnormality was defined in the superior and inferior halves of the patients' reflectance findings, when the fraction of enface slab showing reflectance abnormality (described above) was greater than the ninety-fifth percentile of fractions found in the controls. On the cRNFLT measure, abnormality was defined when the cRNFLT of the sector under consideration less than fifth percentile of the controls.

When the cRNFLT measure of a subject showed glaucomatous abnormality but reflectance findings did not, we re-extracted the enface images in steps of 4 μm from 0 μm to 120 μm. This was to investigate whether there were any reflectance defects we may have missed because of the relatively thick slab-images analysed, or the choice of depths at which the slab-images were extracted.

Results

As shown in *Table 1*, the controls and patients with glaucoma had similar axial lengths and refractive errors, and the controls were on average slightly younger than the patients. As shown in *Figure 3*, the findings of glaucomatous abnormality were consistent (absolute agreement) with the reflectance findings in 26 of the 33 patients studied. There was a strong correlation between the reflectance findings of the entire enface slab-image region studied and the corresponding cRNFLT sector measure, $r_s(31) = -0.82$ with $p < 0.001$ (*Figure 3*).

For the sectorial comparisons (*Figure 4*), absolute agreement was found in 27/33, for both ST and IT findings. There were strong correlations between the superior and inferior regions of the enface slab-images and their corresponding ST and IT cRNFLT measures, $r_s(31) = -0.74$ and $r_s(31) = -0.75$ respectively, both with $p < 0.001$. The kappa values assessing the agreement for the ST and IT findings found moderate agreement, 0.53 and 0.57 respectively (*Figure 4*).

Table 1. Summary descriptive statistics for the subjects studied

	Controls	Patients with glaucoma
Number of subjects	31	33
Age (mean, S.D.) in years	61, 9	69, 8
Axial length (mean, S.D.) in mm	24.6, 1.1	24.2, 1.4
Equivalent spherical refractive error (mean, S.D.) in dioptres	−1.50, 2.25	−1.00, 2.5
MD (mean, S.D.) in dB	–	−3, 3
Global cRNFLT (mean, S.D.) in μm	95, 10	70, 11

cRNFLT, circumpapillary retinal nerve fibre layer thickness; MD, perimetric mean deviation; S.D., standard deviation.

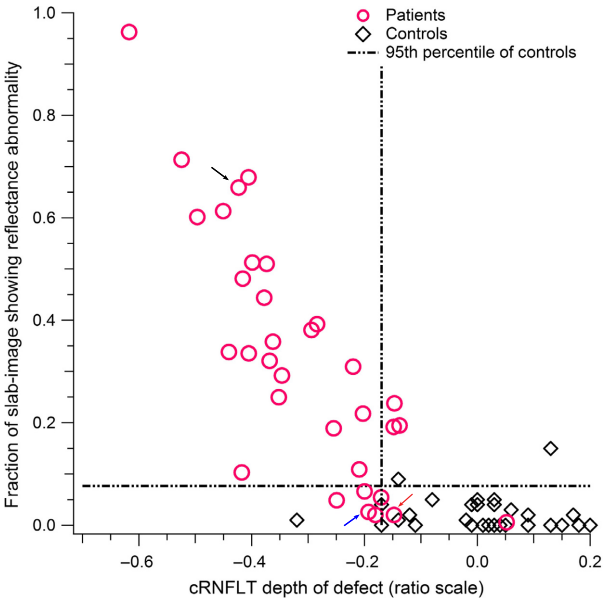

Figure 3. The relation between the reflectance findings for the entire slab-image area studied vs the temporal half circumpapillary retinal nerve fibre layer thickness (cRNFLT) measure, in the patients with glaucoma. The arrows point to the findings for subjects whose enface images and nerve fibre layer thickness profiles are shown in *Figures 5–7*.

An example of a subject for whom both the reflectance findings and the cRNFLT findings agreed for both the ST and IT sectors is illustrated in *Figure 5*. *Figures 6* and *7* show examples of subjects with discordance between the cRNFLT findings and the enface slab-image findings.

Discussion

There is growing interest in the potential use of the enface visualisation of the RNFL reflectance to enhance clinical information for diagnosing and managing glaucoma.[1,2] In

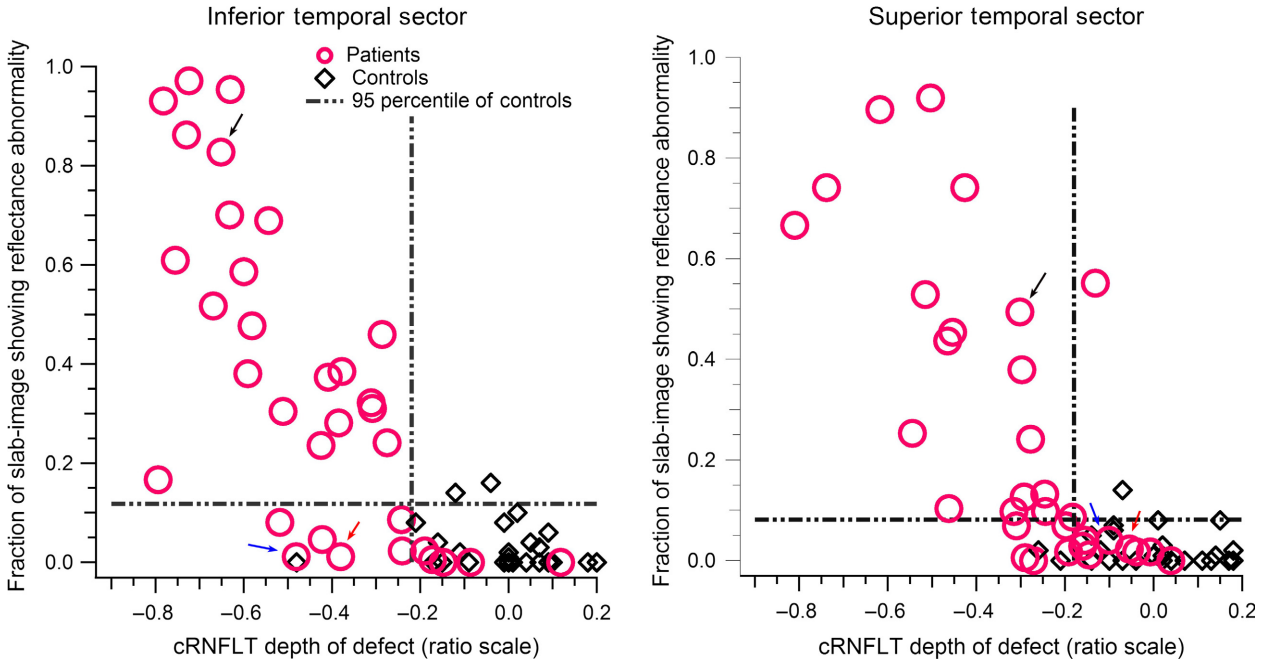

Figure 4. The relation between the slab-image reflectance findings and circumpapillary retinal nerve fibre layer thickness (cRNFLT) findings, for the superior temporal and inferior temporal disc sectors. The arrows point to the findings for subjects whose enface images and nerve fibre layer thickness profiles are shown in *Figures 5–7*.

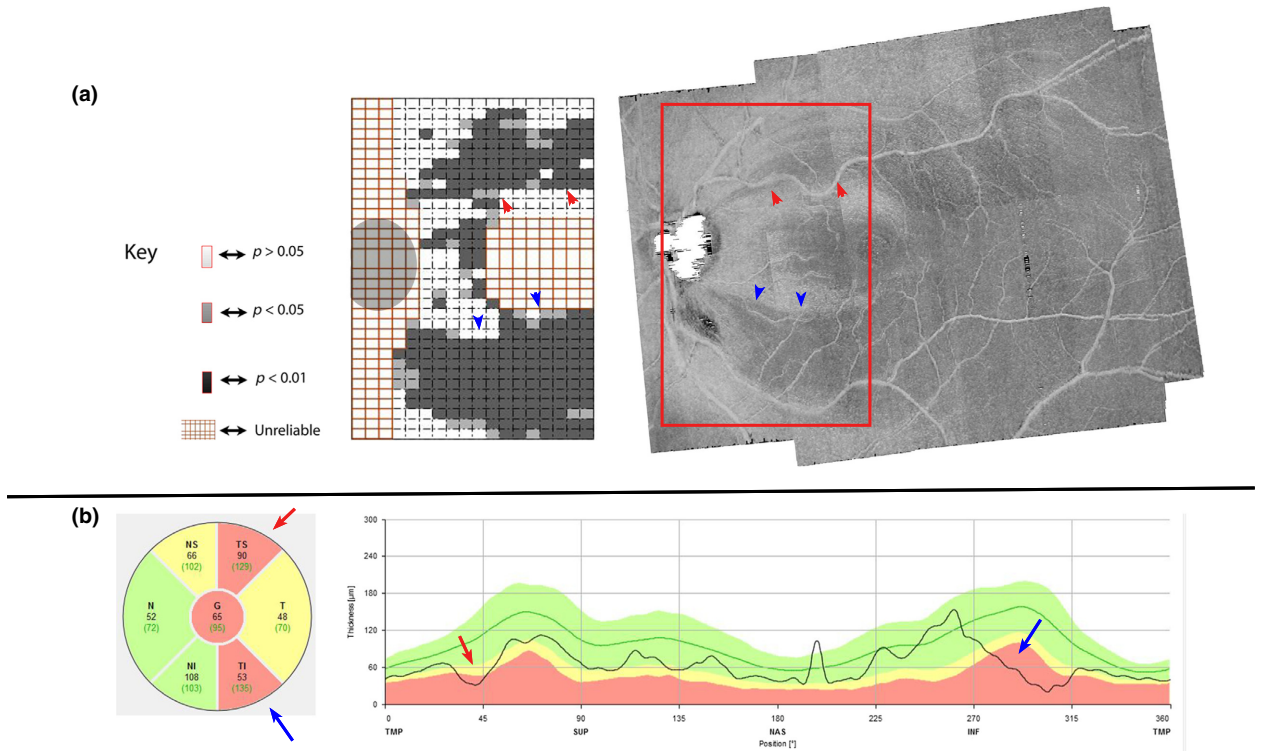

Figure 5. Agreement between circumpapillary retinal nerve fibre layer thickness (cRNFLT) thickness finding, and slab-image reflectance findings, in a patient with glaucoma. (a) Enface slab-image and a corresponding reflectance probability map showing both superior temporal (ST) and inferior temporal (IT) abnormality. (b) cRNFLT profile with IT and ST abnormalities. The subject is identified with a black arrow in *Figures 3* and *4*.

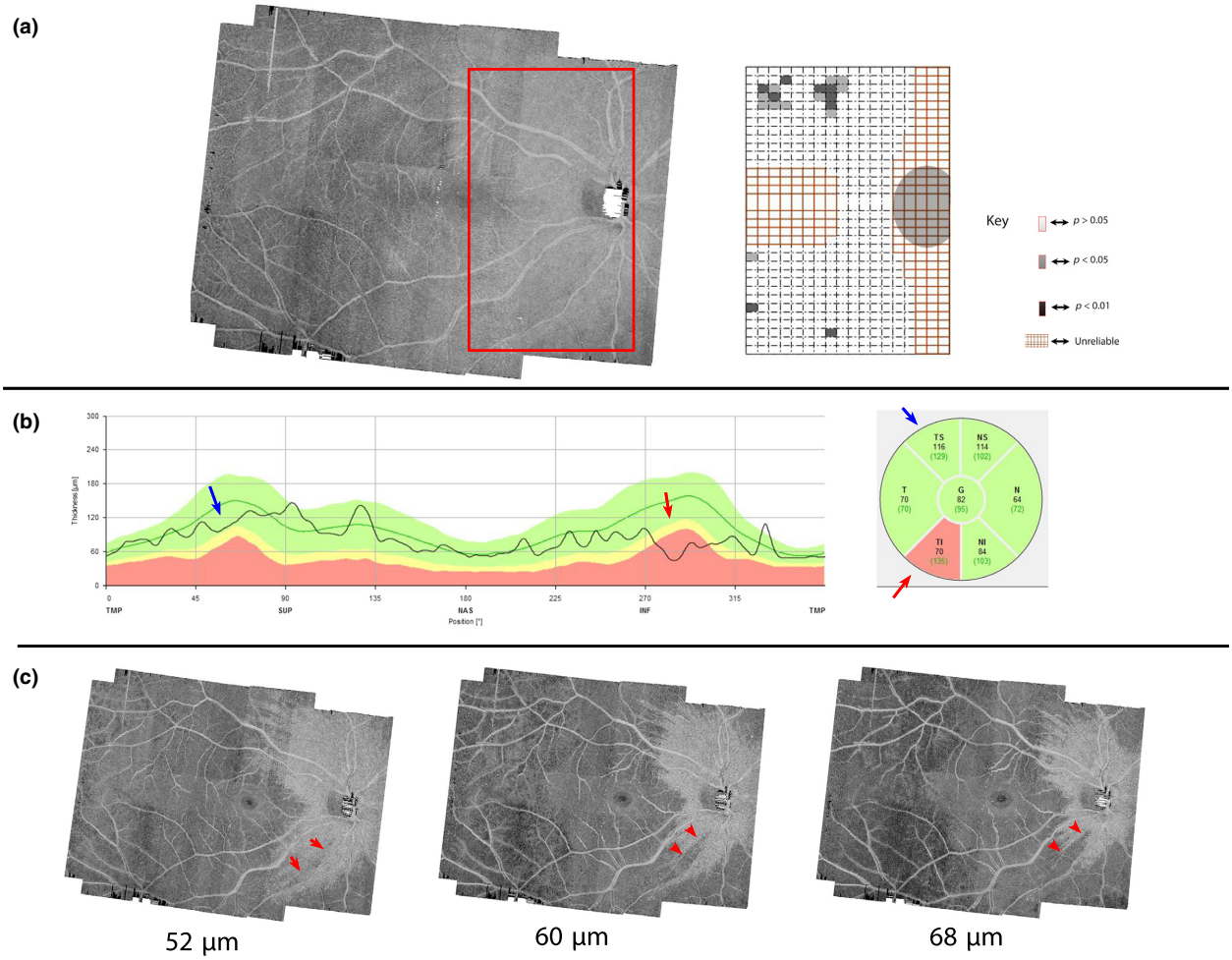

Figure 6. A subject with noticeable circumpapillary retinal nerve fibre layer thickness with inferior temporal (cRNFLT IT) abnormality but without a slab-image abnormality. (a) Enface slab-image and a corresponding probability map. (b) cRNFLT with IT abnormality. (c) Four micrometre thick slab-images centred at the depths labelling the fibres. The split in RNFB reflectance becomes more obvious at depths deeper than 52 µm. The subject is identified with a blue arrow in *Figures 3* and *4*.

this study, we quantified the reflectance findings on RNFL enface images, and found that the surface areas of the enface images showing reflectance abnormalities strongly correlated with the glaucomatous abnormalities quantified with the cRNFLT protocol. Thus, it is possible to quantify the severity of the glaucomatous abnormality in a clinical population based on the reflectance of the RNFL, and find results comparable to the findings from well-established clinical measures. Appropriate measures must be taken in order to further mitigate the impact of reflectance artefacts, such as presumed glial alteration reflectances, as well as to account for the between-subject variability in the retinal anatomical features. A major potential advantage of quantifying the enface reflectance abnormalities is that they preserve the spatial information concerning the glaucomatous abnormality, and that makes the technique a useful approach for targeted perimetry.[20]

The patterns of the reflectance abnormality we found in the patient group typically followed the trajectory of the nerve fibre bundles to the disc.[2] There were four main patterns (*Figure 8*). These were arcuate cluster-pattern, diffuse cluster-pattern, cluster-pattern distal to the disc, and cluster-pattern proximal to the disc. However, some of the patients with glaucoma, as in the controls, did not show any definable cluster-patterns of abnormality (*Figure 8c*). It was only when we investigated depths deeper than 52 µm (at which the slab-image was terminated) that some reflectance patterns that we suspect to indicate abnormality emerged (*Figures 6* and *7*). In three of the six subjects without any definable cluster-patterns of abnormality, the reflectance abnormality appeared as wedge-like defects localised to deeper depths from the ILM (*Figure 6*). In the other three subjects, the RNFB abnormalities seemed diffuse (without any traces of localised abnormality) so that

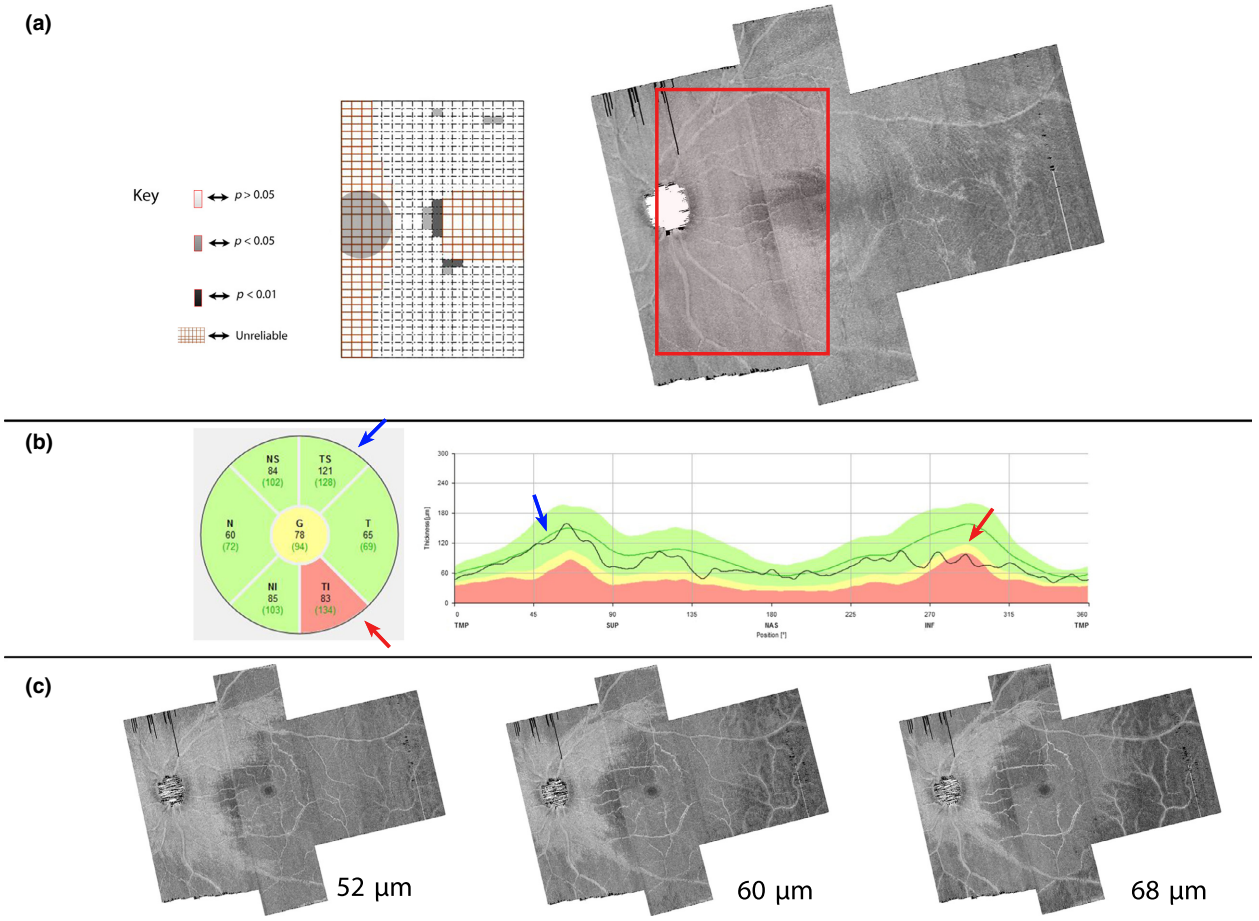

Figure 7. A subject with noticeable circumpapillary retinal nerve fibre layer thickness with inferior temporal (cRNFLT IT) abnormality but without a slab-image reflectance abnormality. (a) Enface slab-image and a corresponding reflectance probability map. (b) cRNFLT finding with IT showing abnormality. (c) Four micrometre thick slab-images centred at the depths labelling the images. No localised reflectance abnormality was seen in the inferior enface region at 52 µm. However, a relatively large reflectance asymmetry in a direction consistent with the cRNFLT abnormality can be seen at deeper depths. The subject is identified with a red arrow in *Figures 3* and *4*.

only a considerable asymmetry in the reflectance of the RNFBs (*Figure 7*) provided an indication of glaucomatous damage. Lateral dispersion of the nerve fibre bundles[21] as they route to the disc may offer some explanation for this phenomenon. If the fibres are widely, laterally dispersed, it may be unlikely that the abnormalities will form a sharp and well-defined arcuate/wedge defect on the enface images. In addition, a generally diffuse loss of the RNFL, such as the inferior hemi-retina of the subject shown in *Figure 7*, may provide some explanation for this phenomenon. We therefore infer that the definition of glaucomatous abnormalities on the enface images should include considerations about the asymmetry of the fibres as well as wedge defects, recognisable only in the deeper retinal layers.

The absence of reflectance abnormalities on the slab-images of some of the patients with glaucoma requires consideration of how to optimally extract slab-images for quantifying/visualising the RNFL reflectances. The previous paper on this topic[2] upon which we based some of our slab-extraction parameters, proposed a few other options. One was to vary the parameters for generating the slab-images across subjects instead of using a fixed slab parameter across subjects. While this is plausible, it is not yet clear how to objectively determine a parameter optimal for determining what the slab-image thickness should be in any given subject. The study by Hood *et al.*[2] used a 52 thick-slab from the ILM across all subjects, which we found to be a straightforward approach that did not require any parameter to determine what the slab-image thickness should be in any particular subject.

Generating the slab-images in the manner used by Hood *et al.*, and now by us, has some advantages. One such advantage is that it requires segmentation of the RNFL only at the ILM-vitreous interface reducing the impact of

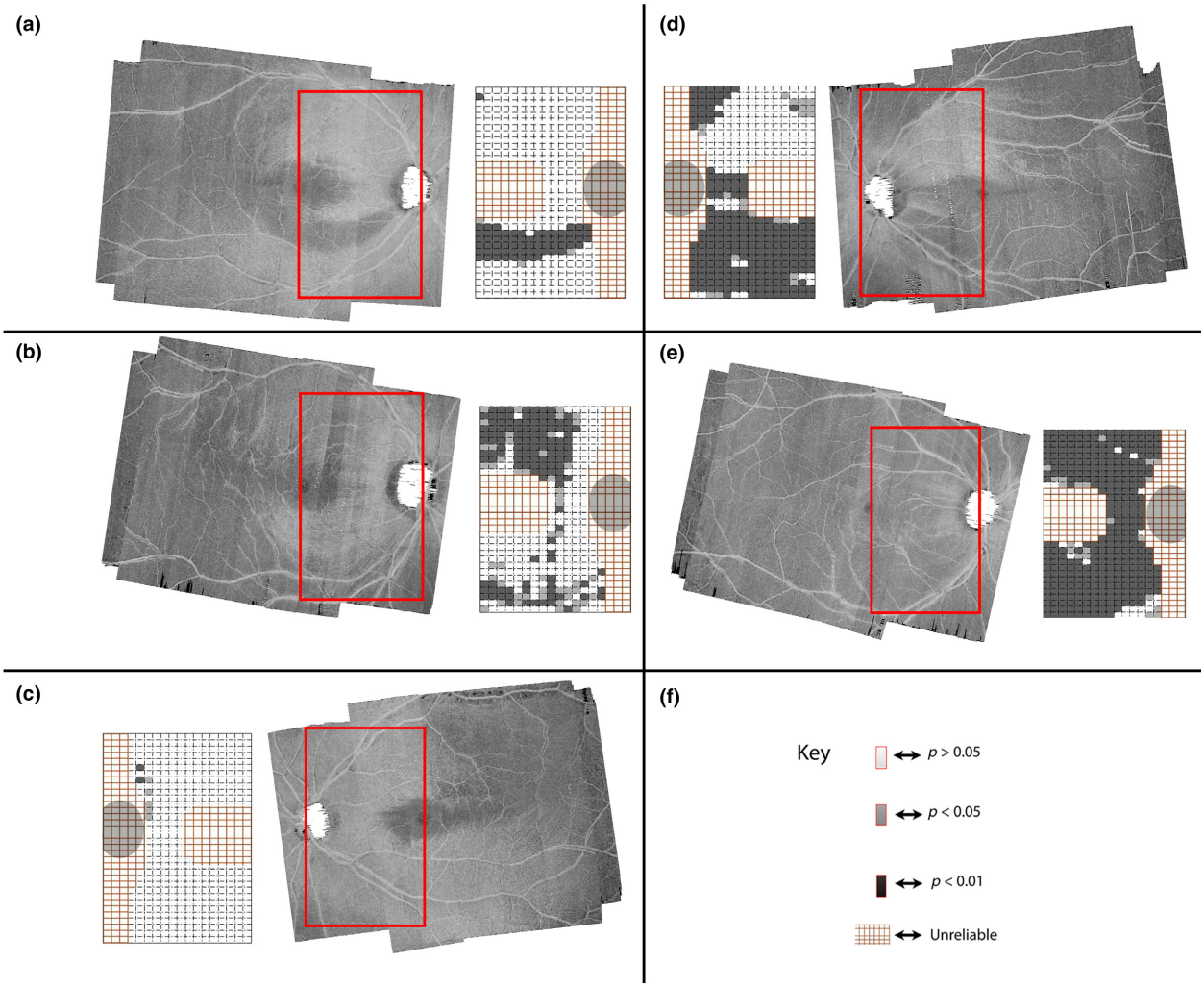

Figure 8. Customised enface slab-images and the categories of reflectance abnormality-patterns found in the patients with glaucoma. Each section shows the region of the enface slab-image studied (in a red box) with a corresponding reflectance probability map. The inferior half of the reflectance probability map of (a) illustrates an arcuate cluster-pattern configuration. The superior half of the probability map of (b) illustrates the cluster-pattern distal to the disc configuration. The superior and inferior halves of reflectance map in (c) illustrate a no-definable cluster-pattern configuration. The superior half of (d) illustrates the cluster-pattern proximal to the disc configuration. The inferior and superior halves of the probability map in (e) shows the diffuse cluster-pattern configuration. (f) The key for the reflectance probability map.

segmentation artefacts, which are likely to be more common at the RNFL/ganglion cell layer interface.[2] The approach also includes information about both the reflectance and thickness of the RNFL because the thicker the RNFL layer the less the less likely the hyporeflective regions beneath the RNFL are included in the slab-image. However, the fact that the abnormalities in some patients were only present in the deeper layers is an invitation to include layers deeper than 52 in the slab-images. Although this could simply be done by including deeper layers in generating the slab-images, it has the potential to weaken the RNFL reflectances quantified in the healthy population. This is because the lower fifth percentile RNFLT measure of the papillomacular bundle, in the healthy population is about 50 μm, based on the cRNFLT machine normative data. The inclusion of thicker slabs, and therefore the less reflective layers beneath the RNFL may affect the ability to detect loss in the patients with glaucoma. A useful approach to dealing with this challenge will be to vary the slab-parameters across the retina as described in our methods, but in addition, vary the slab thickness based on the relative position of the arcades. In the arcades, the lower fifth percentile cRNFLT in the peripapillary region is about 80 μm – based on the cRNFLT machine normative data. Varying the slab-image thickness based on the relative locations of the arcades/papillomacular bundle means the slab-images can

be as thick as 80 μm in the arcade regions. That way the abnormalities localised to the deeper defects in the regions of the arcades (such as shown in *Figures 6* and *7*) can be detected.

On the enface slab-images, we noticed pockets of remnant RNFB bundles with close-to- reasonably intact reflectances within the arcuate and diffuse reflectance defects such as shown *Figure 9*, also illustrated in *figure* 5*a* of Hood *et al.*[2] This pattern is consistent with findings that the localised morphological changes in the lamina cribrosa correspond with the retinal regions with glaucomatous abnormality.[22,23] Given that the lamina cribrosa compartmentalises the RNFBs through its pores, it is reasonable to think that structural disturbance altering the pores of the lamina cribrosa can initiate or exacerbate the events that alter axonal transport and axonal cyto-architecture, ultimately leading to a loss on the RNFB reflectivity. On the other hand, the RNFBs routing through less deformed pores could potentially retain their reflectivity.[22,23] A combination of OCT enface visualisation of the RNFL reflectances and OCT-enhanced depth imaging of the laminar pores might provide *in vivo* longitudinal information on the localised deformation of the lamina cribrosa and the associated changes in the reflectance of the RNFBs.[1]

Figure 9. Remnant retinal nerve fibre bundle reflectance within reflectance abnormality. The blue arrows point to remnant fibres on the enface slab-images of two subjects.

Caveats and limitations

Certain limitations would need to be considered while interpreting the results from our study. Firstly, acquiring high density scans necessary for analysing the reflectance of the RNFBs (such as done in this study) relies on the proficiency of the ophthalmic technician imaging the subjects, considerable cooperation by the subject being imaged, relatively clear ocular media, and a favourable ocular surface condition. Our technique also relies on an image processing tool to provide attenuation coefficients that reduce the impact of reflectance artefacts that may affect the reflectivity of the RNFBs, such as shadows caused by vitreal floaters. In instances where any one of these is compromised, the measured reflectance of the RNFB may be affected. Further studies will be needed to understand the factors, which affect the reflectivity of the RNFBs on the OCT enface images and how to compensate for them.

Furthermore, although we endeavoured to reduce between-subject variability in the disc-fovea angle on our analysis by rotating the images, eyes with the different disc-fovea angles are not likely to simply rotate, but also the trajectory of the RNFL to the disc may also be variable. Thus, future studies may need to develop techniques for compensating for these factors as well. In addition, we resolved the differences between the disc-fovea distances by using a standard grid width, dictated by the subject with the shortest disc-fovea distance across all subjects studied. This limited the surface area within which the RNFL reflectance abnormalities could be assessed especially in subjects with larger disc-fovea distances. A potential strategy for dealing with this would be to apply a magnification factor to the images to compensate for the between-subject variability in the disc-fovea distance, or to stratify the normative data based on the disc-fovea distances so that the subjects can be matched based on the disc-fovea distance.

Another shortfall to consider is the spatial limitations in comparing the enface images to the cRNFLT. We compared the inferior halves and superior halves of the enface images to the IT and ST cRNFLT measures, respectively. This means that on the enface images, approximately one half of the region covered by the pappillomacular bundle was included in the enface regions, compared to the ST and IT cRNFLT disc measures which may contain little to none of the papillomacular bundle. The potential relation between

the ST and IT cRNFLT findings and the enface area with abnormality can therefore be improved by optimising the spatial correspondence between the two measures. A potential way to deal with this is to have a human observer delineate which boxes on the grid map onto the IT and ST cRNFLT disc sectors, although this strategy also has its limitations.

While our technique generates encouraging results for quantifying the enface visualisation of the RNFL reflectance, the results also suggest some weaknesses that can be addressed by further refinements.

First, the findings of the analysis technique may be enhanced by compensating for the directional reflectivity of the RNFBs.[9] The directional reflectivity of the bundles also has the potential to affect the test-retest variability of the technique because the position of the imaging beam through the pupil is not likely to be the same between two different imaging sessions.

Second, the size of the grid boxes used in this analysis can be optimised. Given that the width of the abnormalities gets smaller as the defect approaches the disc, it may be necessary to adapt the grid box sizes for analysing the images based on its relative position from the disc so that mild abnormalities, which form small defects in the region of the disc, can still be resolved by the quantifying analysis.

Conclusion

To conclude, enface RNFL reflectances can be quantified and the results yield valuable clinical information in a manner similar that obtained by cRNFLT measures. The large surface area of the RNFL assessed by the enface visualisation of the RNFL and the ability to quantify the reflectance abnormalities on the enface images hold promise for automating techniques for sampling the retina in targeted perimetry. In addition, the definition of glaucomatous abnormalities in the enface visualisation of the RNFL reflectances should not only be limited to localised arcuate/wedge defects or obvious diffuse losses in the RNFL superficial layers but should include considerations of reflectance asymmetry in the deeper retinal layers.

Acknowledgement

This research was supported by grants from the National Institutes of Health: NIH R01EY024542, 5P30EY019008.

Disclosures

The authors Ashimatey, King and Burns report no conflicts of interest and have no proprietary interest in any of the materials mentioned in this article. The author Swanson reports the following commercial relationships: Consultant, Heidelberg Engineering; and Consultant, Carl Zeiss Medictec.

References

1. Fortune B. In vivo imaging methods to assess glaucomatous optic neuropathy. *Exp Eye Res* 2015; 141: 139–153.
2. Hood DC, Fortune B, Mavrommatis MA *et al.* Details of glaucomatous damage are better seen on OCT en face images than on OCT retinal nerve fiber layer thickness maps. *Invest Ophthalmol Vis Sci* 2015; 56: 6208–6216.
3. Chauhan BC, Sharpe GP & Hutchison DM. Imaging of the temporal raphe with optical coherence tomography. *Ophthalmology* 2014; 121: 2287–2288.
4. Bedggood P, Nguyen B, Lakkis G, Turpin A & McKendrick AM. Orientation of the temporal nerve fiber raphe in healthy and in glaucomatous eyes. *Invest Ophthalmol Vis Sci* 2017; 58: 4211–4217.
5. Tanabe F, Matsumoto C, McKendrick AM, Okuyama S, Hashimoto S & Shimomura Y. The interpretation of results of 10-2 visual fields should consider individual variability in the position of the optic disc and temporal raphe. *Br J Ophthalmol* 2018; 102: 323–328.
6. Patel NB, Luo X, Wheat JL & Harwerth RS. Retinal nerve fiber layer assessment: area versus thickness measurements from elliptical scans centered on the optic nerve. *Invest Ophthalmol Vis Sci* 2011; 52: 2477–2489.
7. Alluwimi MS, Swanson WH, Malinovsky VE & King BJ. A basis for customising perimetric locations within the macula in glaucoma. *Ophthalmic Physiol Opt* 2018; 38: 164–173.
8. Huang XR, Zhou Y, Kong W & Knighton RW. Reflectance decreases before thickness changes in the retinal nerve fiber layer in glaucomatous retinas. *Invest Ophthalmol Vis Sci* 2011; 52: 6737–6742.
9. Huang XR, Knighton RW, Feuer WJ & Qiao J. Retinal nerve fiber layer reflectometry must consider directional reflectance. *Biomed Opt Express* 2016; 7: 22–33.
10. Knighton RW & Huang XR. Directional and spectral reflectance of the rat retinal nerve fiber layer. *Invest Ophthalmol Vis Sci* 1999; 40: 639–647.
11. Ashimatey BS, King BJ & Swanson WH. Retinal putative glial alterations: implication for glaucoma care. *Ophthalmic Physiol Opt* 2018; 38: 56–65.
12. Graf T, Flammer J, Prunte C & Hendrickson P. Gliosis-like retinal alterations in glaucoma patients. *J Glaucoma* 1993; 2: 257–259.
13. Grieshaber MC, Moramarco F, Schoetzau A, Flammer J & Orguel S. Detection of retinal glial cell activation in glaucoma by time domain optical coherence tomography. *Klin Monbl Augenheilkd* 2012; 229: 314–318.
14. Swanson WH, Malinovsky VE, Dul MW *et al.* Contrast sensitivity perimetry and clinical measures of glaucomatous damage. *Optom Vis Sci* 2014; 91: 1302–1311.
15. Vermeer KA, Mo J, Weda JJ, Lemij HG & de Boer JF. Depth-resolved model-based reconstruction of attenuation

coefficients in optical coherence tomography. *Biomed Opt Express* 2013; 5: 322–337.
16. Girard MJ, Strouthidis NG, Ethier CR & Mari JM. Shadow removal and contrast enhancement in optical coherence tomography images of the human optic nerve head. *Invest Ophthalmol Vis Sci* 2011; 52: 7738–7748.
17. Vrabec F. The temporal raphe of the human retina. *Am J Ophthalmol* 1966; 62: 926–938.
18. Huang G, Gast TJ & Burns SA. In vivo adaptive optics imaging of the temporal raphe and its relationship to the optic disc and fovea in the human retina. *Invest Ophthalmol Vis Sci* 2014; 55: 5952–5961.
19. Ashimatey BS, Brett KJ, Malinovsky VE & Swanson WH. Novel technique for quantifying retinal nerve fiber bundle abnormality in the temporal raphe. *Optom Vis Sci* 2018; 95: 309–317.
20. Alluwimi MS, Swanson WH, Malinovsky VE & King BJ. Customizing perimetric locations based on en face images of retinal nerve fiber bundles with glaucomatous damage. *Transl Vis Sci Technol* 2018; 7: 5. doi:10.1167/tvst.7.2.5
21. Ogden TE. Nerve fiber layer of the macaque retina: retinotopic organization. *Invest Ophthalmol Vis Sci* 1983; 24: 85–98.
22. Tatham AJ, Miki A, Weinreb RN, Zangwill LM & Medeiros FA. Defects of the lamina cribrosa in eyes with localized retinal nerve fiber layer loss. *Ophthalmology* 2014; 121: 110–118.
23. Quigley HA, Hohman RM, Addicks EM, Massof RW & Green WR. Morphologic changes in the lamina cribrosa correlated with neural loss in open-angle glaucoma. *Am J Ophthalmol* 1983; 95: 673–691.